communications biology

Article

https://doi.org/10.1038/s42003-024-07160-y

The brain's first "traffic map" through Unified Structural and Functional Connectivity (USFC) modeling

Check for updates

Arzu C. Has Silemek [1,2] ✉, Haitao Chen [2,3], Pascal Sati [1,2] & Wei Gao [2,4] ✉

The brain's white matter connections are thought to provide the structural basis for its functional connections between distant brain regions but how our brain selects the best structural routes for functional communications remains poorly understood. In this study, we propose a Unified Structural and Functional Connectivity (USFC) model and use an "economical assumption" to create the brain's first "traffic map" reflecting how frequently each segment of the brain structural connection is used to achieve the global functional communication system. The resulting USFC map highlights regions in the subcortical, default-mode, and salience networks as the most heavily traversed nodes and a midline frontal-caudate-thalamus-posterior cingulate-visual cortex corridor as the backbone of the whole brain connectivity system. Our results further revealed a striking negative association between structural and functional connectivity strengths in routes supporting negative functional connections, as well as significantly higher efficiency metrics and better predictive performance for cognition in the USFC connectome when compared to structural and functional ones alone. Overall, the proposed USFC model opens up a new window for integrated brain connectome modeling and provides a major leap forward in brain mapping efforts for a better understanding of the brain's fundamental communication mechanisms.

As of now, the two main non-invasive imaging approaches for characterizing the brain's connectome are: structural diffusion-weighted MRI[1] and resting state functional MRI (rs-fMRI)[2]. Structurally, diffusion-weighted MRI-based tractography approach offers a global view of how distant brain regions are connected through white matter fiber tracts[3]. The human brain's structural connectome is remarkable for its highly organized and modular architecture, facilitating efficient communication and functional specialization[4,5]. Functionally, the resting-state fMRI approach offers a way of measuring "functional connectivity (FC)" by quantifying the degree of blood oxygen level dependent (BOLD) signal fluctuation synchronizations between different brain regions[6,7]. Based on the "neurons firing together wiring together" principle[8], FC measures enable the characterization of the human brain functional connectome[9], which is typically organized into distinct networks including the somatomotor[6], visual[10], auditory[11], default mode network (DMN)[12,13], dorsal attention[12], salience[14], and executive control ones[15]. These functional networks are generally believed to directly underlie various primary, cognitive, and socioemotional functions[16,17]. Both the structural and functional connectome feature a small-world network topology, characterized by densely locally interconnected clusters of brain regions and critical long-distance "short cuts" and hubs that bridge inter-cluster communication[18,19], providing supports for both segregated and integrated information processing, essential for complex cognitive processes[20].

There are ongoing efforts to unveil the relationships between structural and functional connectomes based on the idea that structural white matter fiber bundles form the foundation for FC or communication[21–28]. Most studies are correlational in nature and their findings support a moderate positive relationship between structural and functional connections (via global modules max (R^2) ≈ 0.1, via local modules R^2 ranging between − 0.01 to 0.42)[24,29,30]. However, it is generally accepted that there is not a one-to-one correspondence between these two types of connections since many functional connections exist between brain regions without direct structural connections[31]. Instead, FC could be mediated by multiple segments of structural connections. Given the interconnected nature of the structural connectome, it is likely that there are multiple structural pathways linking each pair of regions with significant FC without a direct structural link.

[1]Department of Neurology, Cedars-Sinai Medical Center, Los Angeles, CA, USA. [2]Biomedical Imaging Research Institute (BIRI), Cedars-Sinai Medical Center, Los Angeles, CA, 90048, USA. [3]Department of Bioengineering, University of California at Los Angeles, Los Angeles, CA, 90095, USA. [4]Department of Biomedical Sciences and Imaging, Cedars-Sinai Medical Center, Los Angeles, CA, 90048, USA. ✉e-mail: arzu.hassilemek@cshs.org; Wei.Gao@cshs.org

However, it remains unclear how our brain selects the best structural route for a specific functional connection. New insights into this structural-functional coupling mechanism would shed important light on how our brain works in health and disease.

In this study, we liken the brain to a country with different brain regions being different cities, the brain's structural connectome corresponding to the road system, and the functional connectivity strength reflecting the amount of people traveling among different cities. Given that there are different routes from one city to another, how people choose their routes will determine the "traffic map" (i.e., the load of each road segment) of the road system. Under this new framework, the goal of this work is to characterize the "traffic map" and reveal the most heavily used structural segments of the brain, which may bear significant implications for better understanding of both normal brain functioning and diseased conditions. To achieve this, we make one important economical assumption that distance and road condition (translating to anatomical distance and structural connectivity (SC) strength in the brain) are the two most important factors for route selection. Based on this principle, we aim to build the brain's first unified structural and functional connectome (USFC) to uncover its first "traffic map". Employing the model, we identified an asymmetric network of brain "traffic", characterized by a predominance of pathways originating from the subcortical, default-mode, and salience networks as well as a midline frontal-caudate-thalamus-posterior cingulate-visual cortex corridor that acts as the backbone of the global brain communication system. Our results also accentuate the critical role of stronger structural connections in underpinning significant negative FCs, offering fresh perspectives on their functional relevance. Finally, the USFC map exhibits elevated levels of efficiency, modularity, and betweenness centrality, as well as better prediction of cognitive performance in comparison to conventional structural and FC maps, supporting its superiority in modeling the brain's communication efficiency and efficacy. Overall, the USFC model provides a novel framework for modeling the brain's integrated structural and functional pathway system and potentially opens up a new window uncovering the brain's working principles.

Results

The brain's first "traffic map"

The USFC map, characterizing the accumulative "functional load" of each structural connection segment (Fig. 1 and Supplementary Fig. 1a), is visualized in the first column of Fig. 2a while the SC and FC maps were presented in the first columns of Fig. 2b, and c, respectively. To better quantify the global distribution of USFC, SC, and FC weights in each brain region, we calculated the overall regional load of each connectivity type and showed their distribution in middle column of Fig. 2. It is immediately clear that USFC featured a long right tail with a set of regions showing much higher values that the rest of the brain (second column of Fig. 2a and Supplementary Table 1). Based on the interquartile range (IQR) calculation[32], we detected 11 outlier regions (out of the range between the 25th and 75th percentile) with much higher regional USFC values than the rest of the brain, indicating their heaviest involvement in all USFC routes. These regions include the bilateral posterior cingulate gyrus (PCG) in the DMN, thalamus/caudate/pallidum in the subcortical network, dorsolateral cingulate gyrus in the salience network, and left Heschl gyrus [median (IQR): USFC = 48.6 (21.07)] (second column of Fig. 2a & Supplementary Table 1). Two of these outliers (i.e., bilateral thalamus) were also highlighted by SC [median (IQR): SC = 19.3 (8.24)] (second column of Fig. 2b, no other outliers were found for SC), while no outlier was found in FC [median (IQR): FC = 6.69 (4.06)] (second column of Fig. 2c). Consistent with the regional loadings, when examined at network level, the subcortical, the salience and the default-mode network ranked as the top three with highest network-level USFC values (third column of Fig. 2a).

The ten most heavily used structural pathways based on USFC were shown in Fig. 3. Strikingly, the two hubs of the DMN (i.e., the right PCG and orbital part of the superior medial frontal cortex), were involved in 7 out of the top-10 most heavily used USFC pathways (Fig. 3 & Supplementary Table 2). The bilateral caudate and thalamus were involved in 6 out these top 10 pathways. Together with three connections between the PCG and visual regions (i.e., left calcarine, superior occipital gyrus and cuneus), one connection between the caudate and left superior orbital frontal cortex, and another one between the right calcarine and inferior occipital gyrus, the top 10 most heavily USFC pathways feature a clearly defined, along-the-middle-line, anterior-to-posterior backbone corridor connecting medial frontal to caudate to thalamus to medial parietal and to visual regions (Fig. 3 & Supplementary Table 2). When we reconstructed the USFC using the Destrieux atlas, the top ten heavily utilized segments in the USFC retained a similar backbone of default mode, subcortical, visual, and limbic regions, while also engaging additional segments such as salience, dorsal attention, and ventral diencephalon (see Supplementary Fig. 2).

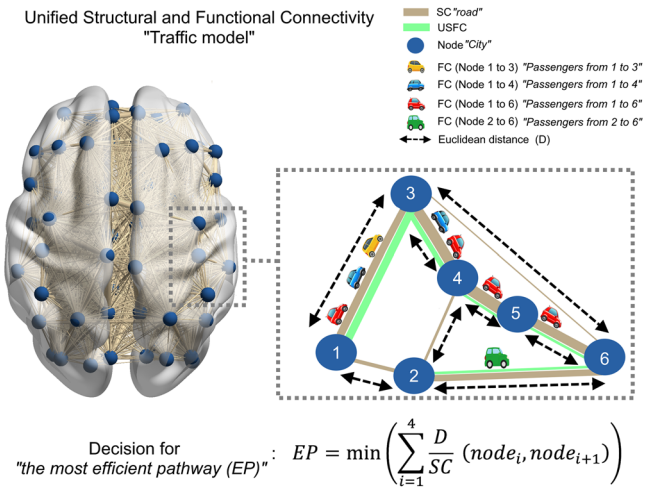

Fig. 1 | "Traffic model" of unified structural and functional connectivity. The left panel shows a glass brain view representing brain network communication. Our approach, on the right magnified image, unifies structural and functional connectivity to depict brain "traffic", likening the brain to a country where each brain region is a city connected by roads (structural connectivity). Passengers (functional connectivity 'cars') choose the most efficient route based on road condition (strength of structural connectivity) and distance. Thicker nude-colored edges between nodes (regions) indicate stronger structural connectivity (better road condition). Black dashed arrows represent Euclidean distances between cities. The right panel illustrates four scenarios with different passengers (functional connectivity 'cars'). The red car chooses a path with 4 steps (1-3-4-5-6) due to much better road conditions over one with shorter distance but much poorer road condition at the last segment (1-3-6). With similar distances, the blue car chooses a path with better road condition (1-3-4) over one with poor road condition (1-2-4). The yellow car opts for a direct/shorter connection with descent road condition (1–3) instead of a longer and inferior route (1-2-4-3). The green car selects the shortest direct link with descent road condition (2–6) rather than a longer route with similar road condition on average (2-4-5-6). The thickness of the green line represents the sum of passengers on each segment. Thicker green lines indicate routes used by more passengers. Equation for the calculation the most "efficient" pathway is given on the bottom of the panel, where EP is the most efficient pathway, D denotes the Euclidian distance and SC reflects the structural connectivity between each pair of AAL connection. "i" indicates the number of steps (up to 4) that are searched to calculate the least cost.

Relationships between SC and FC strengths along the defined USFC routes

To better understand the relationships between SC and FC strengths along the defined USFC routes, correlation analysis was done for USFCs at each step for negative (first column of Fig. 4) and positive FCs (third column of Fig. 4) separately. There are 890/769/3 1-/2-/3-step USFCs supporting positive FCs and 546/1334/42 1-/2-/3-step USFCs supporting negative FCs, as shown in the middle column of Fig. 4, with images from top to bottom

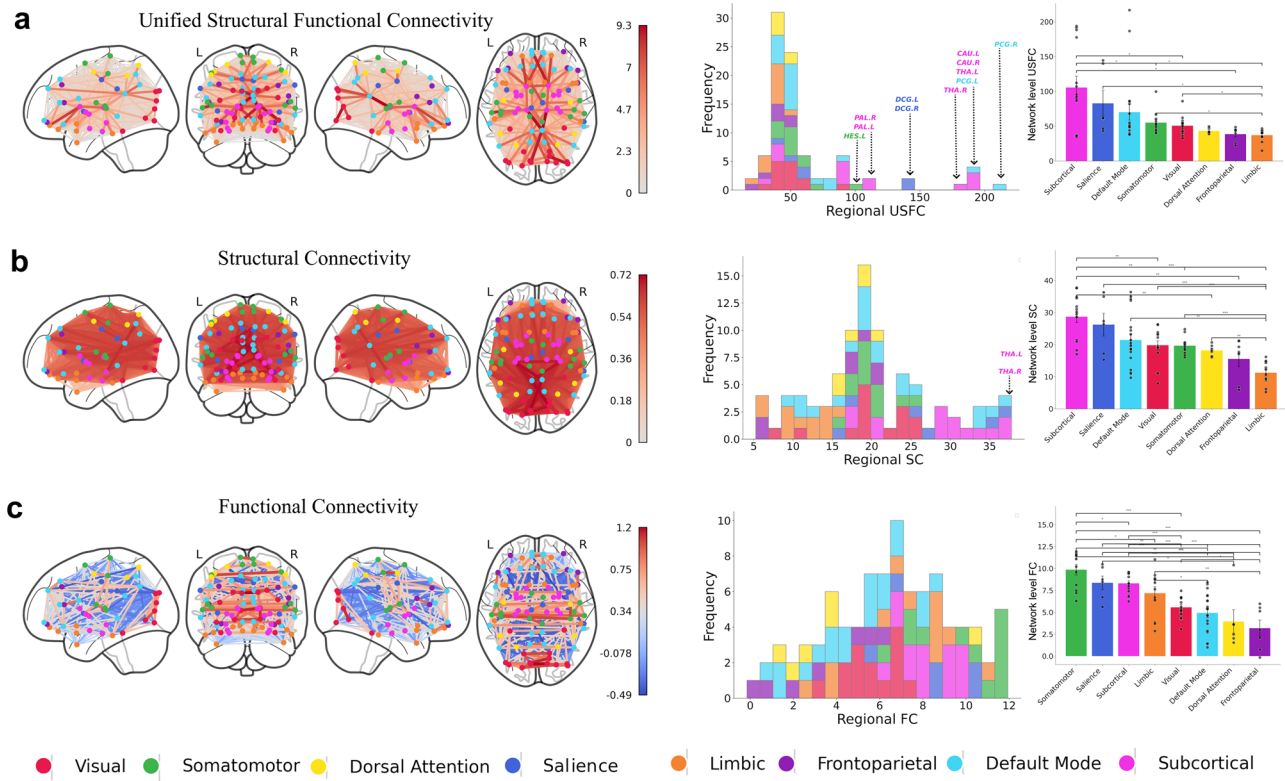

Fig. 2 | Regional and network characteristics of each connectivity type. Each row in panel illustrates glass brain views of the average 'traffic map' weighted by unified structural-functional connectivity (USFC) (**a**), structural connectivity (SC) (**b**), and functional connectivity (FC) (**c**) matrices from top to bottom, respectively. The histograms in the middle column show the frequency distribution of regional USFC (**a**), SC (**b**), and FC (**c**) values. The *x*-axis indicates the sum of connectivity values of each node, and the *y*-axis represents the count of regions within each bin, with bins colored based on the regions' corresponding network involvement. Outliers in USFC (11 regions; HES.L = left Heschl's gyrus, PAL.R and PAL.L = bilateral pallidum, DCG.R and DCG.L = bilateral dorsal cingulate gyrus, THA.R and THA.L = bilateral thalamus, CAU.R and CAU.L = bilateral caudate, PCG.R and PCG.L = bilateral posterior cingulate gyrus) on the histogram (first row of the middle column (**a**)) are labeled based on the Interquartile Range (IQR) (out of the range between the 25th and 75th percentile), with colors indicating the corresponding network. Likewise, bilateral thalamus is labeled via its network color (magenta) as these were found as outliers in regional SC values (second row of the middle column (**b**)). Network-level comparisons are presented in the third column for USFC (**a**), SC (**b**), and FC (**c**), with asterisks denoting significant differences between the networks ($^{*}p < 0.05$, $^{**}p < 0.01$, $^{***}p < 0.001$), and lines indicating standard deviation. Node colors correspond to the respective network as defined by the Yeo Atlas, and bar colors follow the same coding for brain networks. Maps were generated following group-level FDR correction ($p < 0.05$).

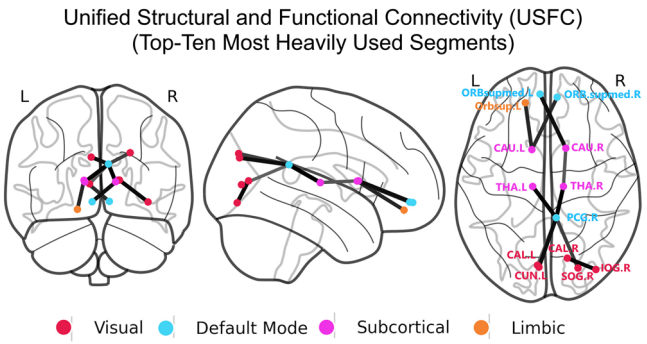

Fig. 3 | Top ten most heavily used segments of an USFC "traffic map". Node colors indicate the relevant network defined by the Yeo Atlas. L = left, R = right, ORBsupmed = orbital part of the superior medial frontal gyrus (blue; default mode network), Orbsup = Orbital part of Superior Frontal Gyrus (orange; limbic network), CAU = caudate (magenta; subcortical), THA = thalamus (magenta; subcortical), PCG = posterior cingulate gyrus (blue: default mode network), CAL = calcarine (red; visual network), CUN = cuneus (red; visual network), IOG = inferior occipital gyrus (red; visual network), SOG = superior occipital gyrus (red; visual network). Edges weighted by USFC values are seen in black.

corresponding to the 1-step, 2-step, and 3-step USFCs, respectively. No common patterns (i.e., shared by >50% of subjects) emerged for 4-step connections so they were not evaluated. For positive FCs, significantly positive (for 1-step routes) (Fig. 4a, third column) or non-significant correlations (for 2 and 3-step routes) (Fig. 4b,c, third column) were observed for routes, which is consistent with previous findings[24]. Intriguingly, more negative FCs were associated stronger SCs for routes underlying negative FCs for all routes raging from 1 to 3 steps (Fig. 4, first column), indicating that stronger negative functional connectivity were supported by USFC routes with stronger structural connectivity (i.e., higher FA). Moreover, the interaction patterns between FCs and SCs, estimated using our novel economical assumption with a different Destrieux atlas, closely reproduced association patterns in our primary analysis—stronger SCs were associated with stronger FCs in magnitude (except for the one-step connections, which became non-significant for negative FCs. However, this is consistent with the weaker negative association observed for one-step connections compared with indirect two- and three-step connections in our primary analysis, see Supplementary Fig. 3).

Information transferring efficiency of USFC

To examine the information transferring property of the USFC map, three graph-theoretical metrics, namely global efficiency, betweenness centrality,

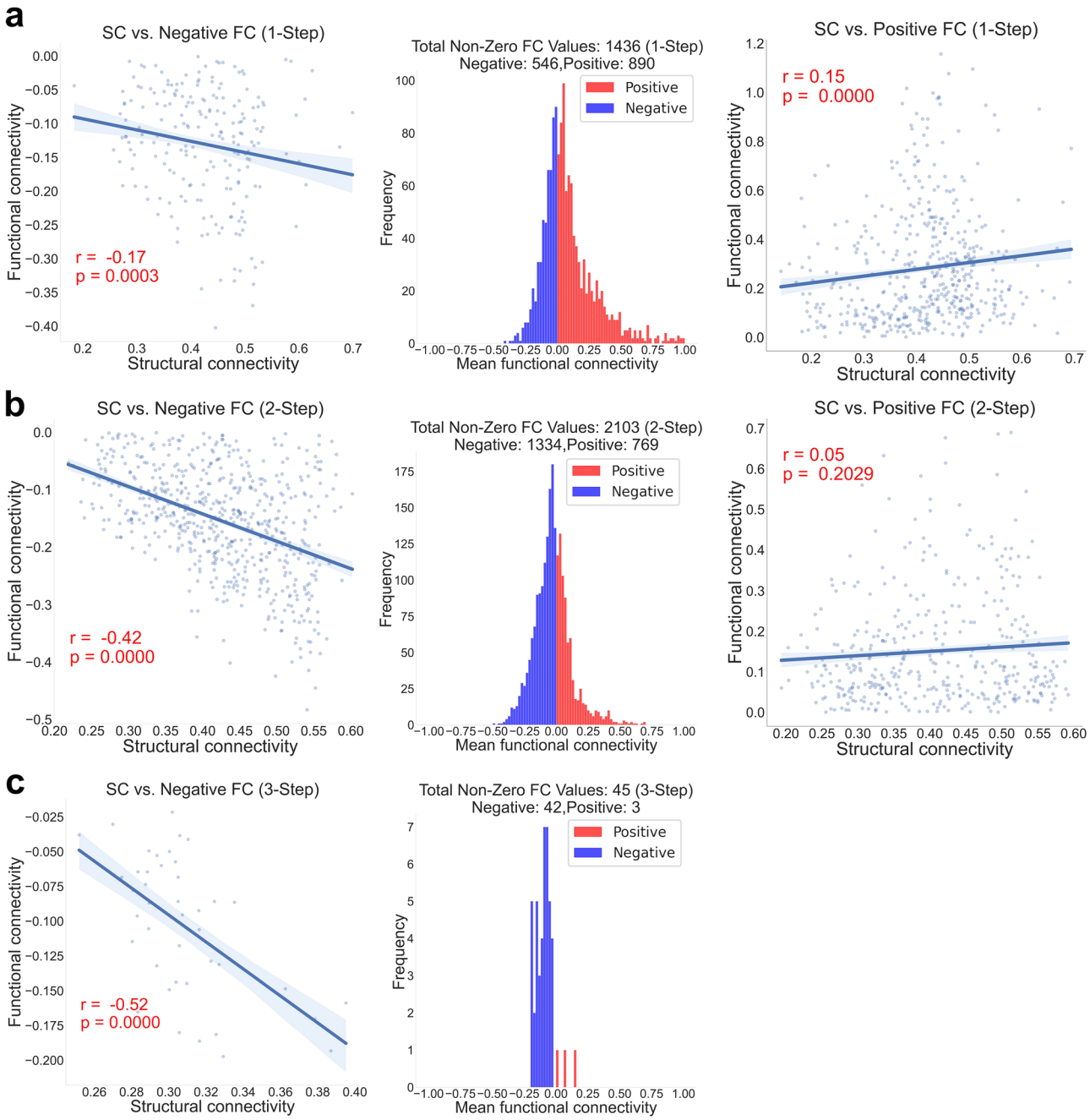

Fig. 4 | Structural and functional coupling in each step. Each row represents the information about functional and structural connectivity within the steps of USFC routes such as 1-Step (**a**), 2-Step (**b**) and 3-Step (**c**). The scatter plots in first column illustrate the relationships between negative functional connectivity (FC) and structural connectivity (SC) for Step 1 (**a**), Step 2 (**b**), and Step 3 (**c**). Similar demonstrations are provided for the coupling between positive FC and SC for each step (i.e., Step 1 (**a**), Step 2 (**b**), and Step 3 (**c**)) on the third column. Distribution plots in the middle column indicate the number of negative (blue) and positive (red) functional connections in each step, such as Step 1 (**a**), Step 2 (**b**), and Step 3 (**c**).

and modularity were calculated and compared between SC, FC, and USFC maps. As shown in Fig. 5, USFC demonstrated superior performances across all three measures, as evidenced by significantly higher global efficiency ($p < 0.001$) (Fig. 5a), betweenness centrality ($p < 0.001$) (Fig. 5b) and modularity ($p < 0.001$) (Fig. 5c). In line with the global measures, significantly superior local efficiency was observed across the entire brain in USFC compared to SC and FC alone (Fig. 5d) ($p < 0.001$). Higher regional betweenness centrality was observed in regions primarily involved in the DMN, as well as in salience, frontoparietal, dorsal attention, limbic, visual and somatomotor networks (Fig. 5e) ($p < 0.001$). Higher local modularity was located in salience, frontoparietal, limbic and subcortical networks (Fig. 5f) in USFC compared to FC and SC ($p < 0.001$). Global efficiency (see Supplementary Fig. 4a) and modularity (see Supplementary Fig. 4b) estimated using the Destrieux atlas remained superior in the USFC compared to FC ($p < 0.001$) and SC ($p < 0.001$) alone. Global betweenness centrality was higher in USFC compared to SC, but lower than FC (see Supplementary Fig. 4c).

Validation of unified structural-functional connectivity in cognitive prediction

To assess the predictive power of USFC for cognitive outcomes, we performed CCA between the top ten heavily utilized segments defined by USFC and fifteen cognitive test scores. USFC demonstrated the highest correlation coefficient compared to SC and FC alone (Fig. 6a). When

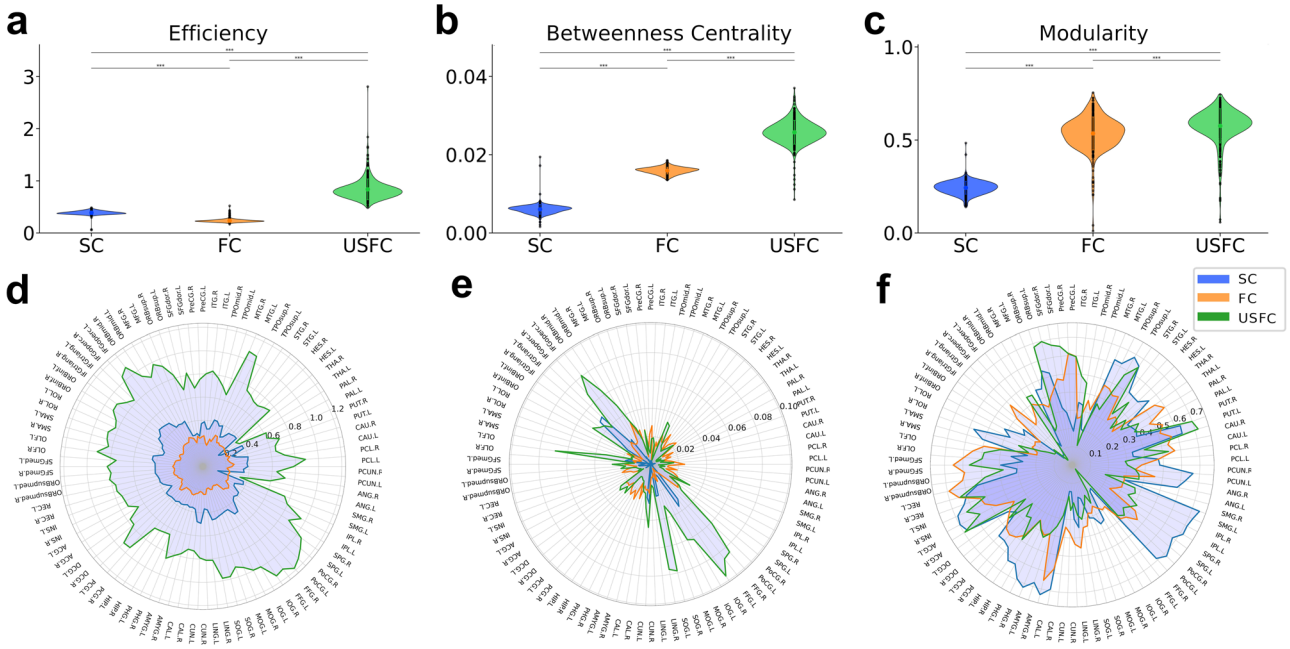

Fig. 5 | Comparative analysis of graph-theoretical metrics across connectivity types. Violin plots depict the distribution of global efficiency (**a**), betweenness centrality (**b**) and modularity (**c**) for unified structural-functional connectivity (USFC, Green), functional connectivity (FC, Orange), and structural connectivity (SC, Blue). Asterisk (***) corresponds to a significant difference between connectivity types (*t*-test, $p < 0.001$). Dots indicate the mean of a specific graph metric for each connectivity type. Lines represent the standard deviation. Radar plot representing the nodal efficiency (**d**), betweenness centrality (**e**) and modularity (**f**) across 90 brain regions for three different connectivity types: SC, FC, and USFC. Each axis of the radar plot corresponds to a distinct brain region, and the distance from the center to a point on a line represents the graph-theoretical metric value for that region. The SC (blue), FC (orange), and USFC (green) connectivity types are depicted as separate lines, allowing for a direct comparison of nodal efficiency across different types of connectivity within each brain region.

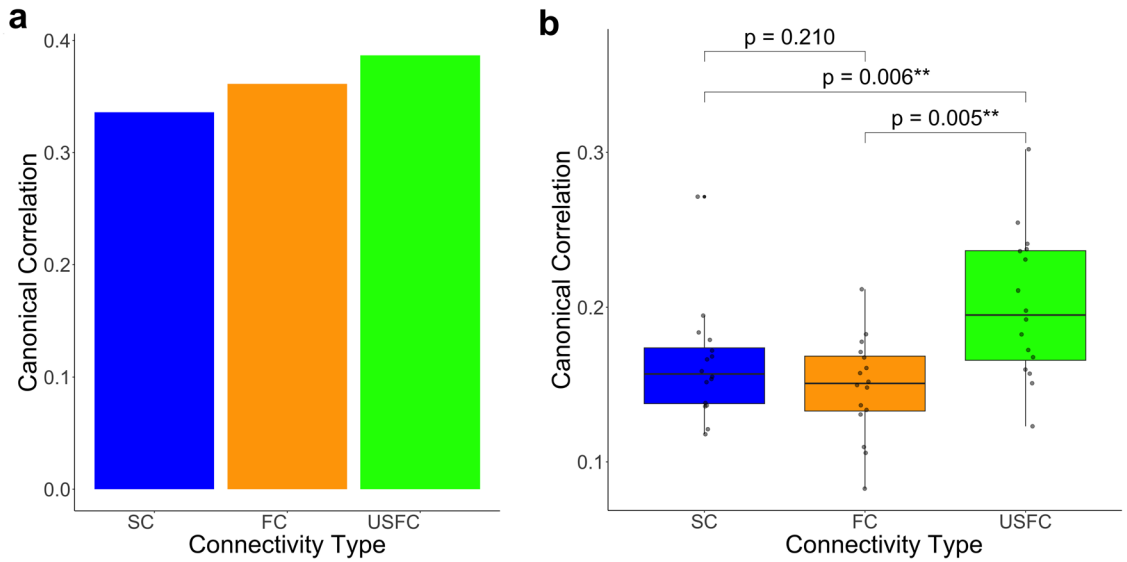

Fig. 6 | Comparison of cognitive associations for structural connectivity (SC), functional connectivity (FC), and unified structural and functional connectivity (USFC) maps. a Bar plot illustrates the correlation coefficients obtained from Canonical Correlation Analysis (CCA) between the top ten most heavily used segments and fifteen cognitive test scores for each metric: SC (blue), FC (orange), and USFC (green). **b** Box plots demonstrate the pair-wise comparison of 15 CCA correlation coefficients between the top ten most heavily used segments and 15 cognitive test scores (done individually) among the three metrics SC (blue), FC (orange), and USFC (green). *P*-values indicate the results of paired *t*-tests comparing pairs of CCA coefficients between FC and SC ($p = 0.210$), between FC and USFC ($p = 0.005$), and between SC and USFC ($p = 0.006$) with asterisks denoting significant differences (*$p < 0.05$, **$p < 0.01$, ***$p < 0.001$).

quantifying the variance explained by the different connectivity models in relation to cognitive outcomes, the USFC model accounted for the highest variance, with the first canonical component explaining ~14.95% of the variance in cognitive scores. In contrast, the FC and SC models explained 13.05% and 11.28% of the variance, respectively. Moreover, when we conducted CCA for each cognitive test and performed a paired *t*-test to examine the significant comparisons between each metric, USFC showed significantly higher correlation coefficients than both FC ($p = 0.005$) and SC ($p = 0.006$) (Fig. 6b). No significant difference was found between SC and FC ($p = 0.210$) (Fig. 6b). These findings suggest

that USFC is more strongly associated with cognitive performance than the other models.

Discussion

Based on an economical assumption, our new Unified Structural and Functional Connectivity (USFC) modeling represents the first effort to build the brain's first "traffic map" highlighting the brain's major structural pathways that are most heavily used for efficient functional signal transferring. Based on this model, we revealed a highly skewed brain "traffic" system featuring the subcortical, the default-mode, and the salience network housing some of the brain's most traversed nodes and a medial frontal-caudate-thalamus-posterior cingulate-visual cortex midline "backbone" corridor as the mostly heavily used structural pathways. Moreover, the finding that stronger structural connections are underlying stronger negative functional connections further supports the functional roles of negative FCs and provides a fresh perspective on the dynamic interactions among brain regions. Finally, the significantly higher efficiency, modularity, and betweenness centrality, as well as the better prediction of cognition demonstrated in the USFC map when compared with structural and functional connectomes, may support the superiority of this "traffic map" in potentially revealing the true working mechanism of the human brain. Overall, the proposed USFC model potentially opens a new window for brain connectome modeling by offering a more intricate depiction of the brain's connectivity landscape based on an inherently multi-modal and integrated modeling of both structural and functional connections.

The Unified Structural and Functional Connectivity (USFC) model presented in this study addresses a critical limitation in the field of brain connectivity modeling with its unique multi-model design and inherent FC-SC integration in its formula of USFC derivation. In contrast, most traditional approaches, including betweenness centrality, k-shortest paths, information efficient paths, as well as others based on graph theory[33–40], treat structural and functional connectivity as separate entities, resulting in a model-specific understanding of brain communication mechanisms, which is often then mitigated by post-hoc FC-SC correlation analysis to characterize their relationships. By integrating these two modalities throughout the process, the USFC model provides a more holistic view of the brain's combined functional and structural connectivity system, overcoming the limitation of considering SC and FC in isolation. Specifically, the fundamental assumption of USFC is that functional communication between any pair of regions is realized through selecting the most efficient (i.e., shortest and strongest) structural pathways. Therefore, the calculation of USFC starts from the FC matrix which defines all pairs of regions with significant functional connectivity. After finding the most efficient structural pathway of each significant functional connection with a combined consideration of both shorter anatomical distance and better signal transferring capacity (i.e., indexed by higher FA), the cumulative functional communication carried by each structural segment across all functional connections is then calculated (i.e., the sum of all functional connection strengths passing through this segment) as the USFC of that segment, representing its actual "traffic load". Therefore, the definition of USFC is inherently FC-driven and multi-modal by combining both structural connectivity and functional connectivity in this well-defined formula. Overall, USFC provides a novel and more integrated understanding of brain networks and allows for the modeling of brain connectivity based on both the anatomical pathways and the functional communication between regions. To the best of our knowledge, no previous methods[41,42] have combined SC and FC in such an integrated manner to derive a combined index of brain connectivity depicting the functional load of each structural connection.

Our analysis uncovered an striking pattern within the brain's USFC blueprint: the DMN regions collectively possess the third highest nodal USFC values while more strikingly, seven of the top ten most heavily trafficked pathways involve either the PCG or medial prefrontal cortex, the two hub regions of the DMN[43]. Centrally located and occupy a large portion of the brain, the DMN is known for being "active" during rest and its versatile roles in self-reference, social cognition, episodic and autobiographical memory, language, sematic memory, among others[44–46]. All these functions involve complex communications within and between DMN and other brain regions which likely underlies our finding of its central role in the newly defined USFC system. Specifically, the prominent inter-network connections between the DMN hubs and subcortical/visual regions as shown in the top ten USFC pathways likely underscore the DMN's potential integrative role across different domains, which is highly in line with findings demonstrating DMN's active and dynamic reorganization of its connectivity patterns across a range of cognitive and socioemotional tasks[47–50]. This finding provides another critical piece of evidence from a global brain "traffic map" perspective that the DMN's role likely goes beyond a passive default state but rather globally contributes to the brain's efficient signal processing across task domains[48,49]. Overall, our finding of the central role of the DMN in the newly defined USFC system provides new support/explanation for its established importance in development[49,51], normal adult functioninXXX12g[47–50,12,52,53], aging[54,55] and various brain disorders[56–59].

Beyond DMN connections, six of the top-ten most heavily trafficked segments involve the thalamus/caudate while at a network level, the subcortical and salience network regions collectively rank as the two mostly traversed networks in the whole brain "traffic map" ranking (Fig. 2). Regarding the salience network, although not highlighted in the top ten mostly heavily used pathways, its regions collectively rank second in the whole brain "traffic map" system and the middle cingulate cortex was detected as one of the "outliers" with the highest USFC loadings. These findings are consistent with its reported role of lying on the apex of the brain's global coordination system by performing a "switching" role among large scale functional networks, especially between the DMN and dorsal attention networks[47,50,60,61].

The subcortical regions, in particular the thalamus's prominence in this "traffic" system is consistent with not only its known role as an "relay center" connecting peripheral neural system with the brain cortices but also its versatile involvement in modulating and refining sensory data, shaping consciousness, and enhancing cognitive functions[62–64]. Its highly utilized connectivity with the PCG may be particularly indicative of a sophisticated mechanism that merges external sensory inputs with internal states, an essential process for coherent cognitive function[65]. Similarly, the caudate nucleus not only plays a critical role in movement planning and execution but also serves in a multitude of essential brain functions, including learning, memory, reward, motivation, emotional regulation, and aspects of romantic interaction[66,67]. Structurally, frontal regions are known to be connected to the caudate, which in turn is connected to the thalamus, and subsequently projecting to PCG[68,69], providing SC support for the observed medial frontal-caudate-thalamus-posterior cingulate -visual pathway that leads the most heavily USFC segments. The finding of a clearly defined midline corridor connecting frontal to caudate to thalamus to posterior cingulate and finally to visual cortices supporting the most "traffic" in the brain through USFC modeling is striking and opens up new windows for better understanding of the "backbone" structure of the brain's global communication system. Consistent with our findings, Hagmann et al. have previously delineated the SC hubs of the human brain and similarly detected a midline "structural core" linking precuneus to posterior, middle, anterior cingulate cortex and finally to medial orbital frontal cortices[4]. However, their examinations exclude subcortical areas so the potential "bridging"/ "disseminating" (e.g., the thalamus) role of subcortical regions were not counted for. With combined consideration of both functional and structural connections and including both cortical and subcortical regions, the midline corridor delineated in this study featuring a frontal-subcortical-parietal-occipital link may have better captured the "backbone" of the brain's global communication system and deserves attention in future search of its relevance in health and disease.

The finding of moderate but significant positive correlations between SC and FC strengths associated with positive FCs is in line with previous reports[24,70]. However, the finding that routes underpinning negative FCs show a robust negative relationship between SC and FC strengths across one-to-three step connections is more intriguing. Ongoing debates

regarding global signal regression and the consequent observation of negative correlations underscore the lack of consensus on a singular method for processing resting state data to uncover the 'true' nature of brain functionality[71]. Contrary to the notion of negative FCs as a mere byproduct of signal processing, emerging research posits it as a salient aspect of the brain's functional architecture defining modularity of the resting-state fMRI connectome, deeply linked with its structural framework[12,72–77]. Our findings add to the evidence supporting the functional significance of negative FCs after global signal regression and suggest that the brain utilizes a delicate traffic system to choose the best routes (i.e., composed of segments with stronger SCs) for negative FCs across different brain regions. Notably, Skudlarski et al. indicated that regions with negative functional FCs are not necessarily disconnected structurally[78]. Instead, there is an implication of a complex relationship where structurally close regions can exhibit negative FCs, suggesting an intricate coordination of brain dynamics. However, we have to point out that the "one-step" route delineated in this study should not be confused with "direct SC" or "connected by a single white matter bundle" given the limitation of diffusion-weighted imaging-based tractography. In other words, the one-step SC used in this study was derived based on probabilistic tractography and as long as there is a "connected structural route" connecting two brain regions, we define these two regions are "structurally connected" and treat them as "one-step" connections. It is possible that multiple white matter fiber bundles are underlying each of these "one-step" structural connection and the accumulated phase lag across the multiple structural connections may have contributed to the observed negative FCs[79]. Compared with the relationships associated with negative FCs, where all three step groups (i.e., 1–3) show significant negative correlations, the relationships associated with positive FCs only show positive relationships for 1-step route. One potential explanation could be that choices for multiple-step positive FCs are more abundant than those for negative FCs, where SC is not necessarily a limiting factor and the choices are not as tightly regulated, resulting in weaker SC-FC correlations. Regardless, the finding that stronger structural routes are underlying stronger negative FCs provides further support for the importance of negative FCs in the brain's integrated communication and functioning.

For all three measures of the brain system communication efficiency, namely global efficiency, modularity, and betweenness centrality, the USFC-based connectome demonstrates significantly higher performance than both the FC and SC systems. These findings support the potential superiority of the USFC system in depicting the brain's signal transferring efficiency. Essentially, only looking at the "road system" (i.e., equivalent to the brain's SC system) or the final "number of people traveling between any two cities" (i.e., equivalent to the brain's FC system) could not provide a clear picture of the brain's underlying "traffic patterns" (since there are multiple pathways linking each pair of cities) while it is this traffic pattern that directly unveils how the road system is used to support the between-city traveling (i.e., signal transferring). The much higher global efficiency and betweenness centrality is likely supported by the most heavily utilized routes between major functional nodes while the higher modularity may result from the more densely connected local systems within USFC. Additionally, the enhanced predictive performance for cognitive functions may indicate that the USFC model integrates both structural and functional information in a manner that better represents the underlying neural mechanisms associated with cognition. This novel way of combined modeling of both structural and functional connections likely allows for a more comprehensive understanding of how different brain regions communicate to support cognitive processes.

Although this work provides a new perspective on brain connectome modeling, there are a number of limitations associated with the current version of USFC that deserve future considerations[80,81]. One important limitation is that the current USFC model does not account for the potential dynamic functional connectivity fluctuations. While the current formula using static FC measures provides an integrated modeling of functional and structural connectivity patterns, it overlooks the potential temporal variability in functional interactions between brain regions[82,83]. Future incorporation of time-dependent functional connectivity[34,82,84], which is known to fluctuate based on cognitive demands, tasks, and internal states[50,85,86] is an important next step so the selection of best structural pathways can also incorporate considerations of the current "real-time" traffic, which may result in better FC-SC modeling. Secondly, functional connectivity as measured by Pearson correlation, reflects statistical associations between brain regions, is prone to noise, common inputs, or indirect connections[87–89], and is inherently limited in its inability to infer causality or directionality between nodes[90]. Therefore, in this manuscript, we used the word "traffic" in quotation marks to facilitate the understanding of our model when we compared it to the real-world traffic system, but this should not be interpreted as FC or USFC indicating direct communication or directed signal flow. Future studies could employ causal modeling approaches such as dynamic causal modeling (DCM) or structural equation modeling (SEM), to better look into the directional relationships between brain regions[81,90]. A third limitation of the USFC model is the assumption that communication always occurs via the shortest and most structurally efficient pathways as previous studies suggested that communication may also unfold through alternative or less economical routes[80,81]. This highlights the need for future work to incorporate additional complexities such as redundancy or probabilistic models in defining network paths to further enhance our understanding of brain connectivity dynamics. Future empirical comparisons with other brain network communication models incorporating path ensembles, dynamic routings, or those beyond shortest paths[80,90] could also further evaluate USFC's relative performance and refine its utility for both theoretical modeling and clinical applications. As mentioned above, direct structural connection in this study might not represent one single fiber bundle. Rather, one-step routes may consist of multiple white matter fiber bundles, which bears critical implications on the understanding of SC-FC relationships, particular those with the negative FCs as detailed above. Moreover, we used average FA along the tracts to index SC strength, but other metrics may also be considered in future development of the model. The FA-weighted connectivity used in this study may not fully capture the complexity of fiber organization in regions with crossing or branching fibers, where FA values can be significantly reduced[91]. This represents a limitation and alternative diffusion metrics, such as Neurite Orientation Dispersion and Density Imaging (NODDI)[92] or spherical deconvolution techniques[93], should be explored in future work to improve structural connectivity modeling in these regions. Finally, while the current CCA analysis provides insights into the relationship between USFC and cognitive performance, future formal prediction analysis incorporating cross-validations may better illustrate generalizability of the detected brain-behavior relationships[94,95].

Overall, by integrating structural pathway properties and functional connectivity strength in a single connectome model, the proposed USFC framework offers a new way of combined modeling of the brain's connectivity system. The end result of an integrated "traffic map" of the whole brain highlighted the critical importance of the subcortical, default-mode, and salience networks, as well as a midline frontal-caudate-thalamus-posterior cingulate-visual cortex "backbone" structure in its global communication system. The higher efficiency measures and better associations with cognitive performances underscore the potential superiority of USFC in modeling this complex and delicately wired system. Future efforts to refine this model and navigate the resulting complex "traffic maps" in both normal and diseased populations may have the potential to transform both theoretical modeling of the brain's connectome and clinical/intervention approaches.

Methods

This study involved 394 subjects from the Human Connectome Project - 1200 Subjects Release (S1200) including behavioral and 3 T MRI data. All research involving HCP young adult data was conducted in accordance with ethical standards established by the Institutional Review Board (IRB) at Washington University in St. Louis and at the University of Minnesota[96]. The data collection protocols were approved by these institutions, ensuring that all

participants provided informed consent prior to participation in the study. This adherence to ethical guidelines guarantees the protection of participant rights and the integrity of the research process. These subjects were randomly selected from the shuffled dataset, constituting one-third of the total sample. We downloaded minimally processed diffusion tensor imaging, T1-MPRAGE and rs-fMRI data to perform structural and FC analysis. Details of the minimal image processing are provided in Glasser et al.[97].

Structural connectivity

Individual structural networks were constructed through the utilization of whole brain probabilistic fiber tracking with MRtrix3 (www.mrtrix.org) within the subject's space as described in Has Silemek et al.[98]. To generate fractional anisotropy (FA) and mean diffusivity maps, we initially applied diffusion tensor fitting to diffusion tensor imaging data, accounting for head motion and eddy currents, and performed skull stripping procedures using FSL's diffusion toolbox[99].

To obtain a precise estimation of the fiber orientation distribution (FOD) during constrained spherical deconvolution, we determined the multi-shell, multi-tissue response functions based on FOD values exceeding 0.7 for white matter and lower that 0.2 for gray matter and cerebrospinal fluid[100]. Subsequently, for fiber construction, we employed probabilistic tractography algorithms, which generated a total of 150,000 fibers, with a minimum length threshold set at 20 mm. Default parameters included a step size of 0.2 mm, a minimum radius of curvature of 1 mm, and an FOD cut-off of 0.1. Seeds for tractography were specified using all voxels from 1 mm dilated white matter masks. The tracking of these seeds was confined by the mask's boundaries and predefined FA or FOD thresholds. Streamlines were mapped onto structural image which was labeled based on the AAL atlas (2009). Following this, we computed the average FA for each fiber tract after estimating the FA values at each point along the fiber's trajectory as an index of the SC strength for this fiber tract. For each pair of nodes, the mean FA of the fibers that intersect both nodes was calculated, ensuring that the number of fibers in the selected vectors of the nodes matched the number of fibers in the tract structure.

Functional connectivity

The preprocessing steps for FC involved several key procedures, including skull stripping using FSL, segmentation of white matter, gray matter, and cerebral spinal fluid via FSL FAST and motion correction with AFNI (participants with framework displacement >0.3 mm and <1000 volumes were excluded), bandpass filtering in the frequency range of 0.01 to 0.1 Hz using AFNI, and spatial smoothing via a Gaussian kernel with a full width at half-maximum of 6 mm, non-linear registration of rs-fMRI images to the Montreal Neurological Institute atlas using ANTs. Following preprocessing, global signal regression was applied to remove the mean gray matter signal. Subsequently, FC was computed by measuring the correlation between the average signals of each pair of 90 regions in the AAL atlas ($p < 0.05$, false-discovery rate (FDR)[101] corrected).

Unified Structural and Functional Connectome (USFC) construction

Construction of USFC was performed by a custom MATLAB script[102] including the following procedures:

Template distance calculation

First, we defined a standard distance map based on the AAL template extracting the anatomical coordinates for designated brain regions, which were sequentially labeled from 1 – 90. Then, the Euclidean distance between the center of mass of each of the 90 region pairs was determined.

Identifying the most "efficient" pathway

The cost function was defined as the Euclidean distance of AAL atlas divided by the strength of direct SC between a pair of regions along all potential routes (up to 4 steps were searched). The most "efficient" pathway for each FC in each subject was identified by summing the cost of each "step" and choosing the one with the least "cost" as follows:

$$EP = \min\left(\sum_{i=1}^{4} \frac{D}{SC}\left(node_i, node_{i+1}\right)\right) \quad (1)$$

where EP is the most efficient pathway, D denotes the Euclidian distance and SC reflects the structural connectivity between each pair of AAL connection. Schematic demonstration of the most "efficient" pathway is visualized in Fig. 1.

Unified structural and functional connectivity (USFC) value calculation

A USFC value for each "road segment"/direct SC was then calculated as the sum of all FC values that use this segment in their respective routes, essentially quantifying the amount of "traffic" on this "road segment" for each subject (i.e., weighted by both the number and degree of "traffic") (Fig. 1). After calculating the mean USFC by averaging the values in each pair of connections across the group, one-sample *t*-test and FDR correction at a threshold $p < 0.05$ were applied.

Structural-functional relationships across all USFC routes

To better understand the relationships between SC and FC along the defined USFC routes, we performed functional-structural strength correlation analysis at the group level across all routes in four subgroups based the number of steps of the corresponding route, focusing on those that are consistent in over 50% of the subjects. The SC for each step was calculated by averaging the SC values for every pair of nodes within the respective route. Spearman correlation was performed to test the relationship between the SC and FC at each step and $p < 0.05$ was accepted as significant.

Graph-theoretical metrics

To examine the information transferring efficiency of the newly derived USFC connectome, we utilized three principal graph-theoretical metrics calculating via Networkx package in Python[103] to assess weighted network characteristics: efficiency[104–106], modularity[107], and betweenness centrality[108]. Efficiency denotes the network's capacity for swift and economical propagation of information. Modularity quantifies the degree to which the network is partitioned into cohesive communities or clusters with dense intra-cluster connections. Betweenness centrality measures the nodes' role in facilitating information flow, thus reflecting their capacity to integrate data across disparate functional regions. These metrics were computed for each individual across the three metrics, namely FC, SC, and USFC, and statistical comparisons were made using *t*-tests.

Testing the robustness of the USFC

To demonstrate the robustness of the USFC methodology, we repeated our analysis using an alternative brain parcellation scheme, specifically the Destrieux atlas with 164 regions (82 per hemisphere)[109].

Association between USFC and cognition

To validate our novel framework, we conducted a USFC-cognition association analysis and compared the results with those obtained from functional connectivity (FC) and structural connectivity (SC), respectively. Specifically, we performed a Canonical Correlation Analysis (CCA)[110] focusing on the brain's key structural-functional pathways, defined as the top ten most prominent segments identified by the USFC model, alongside cognitive assessments available in the HCP dataset. The CCA was executed using the cancor function in R, which identifies pairs of canonical variables that optimally represent the relationships between the top ten USFC measures and cognitive performance scores. A total of fifteen cognitive tests from the NIH Toolbox and the Penn Computerized Neurocognitive Battery (CNB) were included, covering a diverse range of cognitive domains:

Memory: Picture Sequence Memory Test (PicSeq_AgeAdj), Penn Word Memory Test (IWRD_TOT).

Executive Function and Cognitive Flexibility: Dimensional Change Card Sort (CardSort_AgeAdj), Flanker Inhibitory Control and Attention Test (Flanker_AgeAdj).

Language and Vocabulary: Oral Reading Recognition (ReadEng_AgeAdj), Picture Vocabulary Test (PicVocab_AgeAdj).

Processing Speed: Pattern Comparison Processing Speed Test (ProcSpeed_AgeAdj).

Working Memory: List Sorting Working Memory Test (ListSort_AgeAdj).

Composite Cognition Scores: Fluid Composite (CogFluidComp_AgeAdj), Crystallized Composite (CogCrystalComp_AgeAdj), Total Composite (CogTotalComp_AgeAdj), Early Childhood Composite (CogEarlyComp_AgeAdj).

Self-Regulation and Impulsivity: Delay Discounting for $200 at 1 month (DDisc_SV_1mo_200).

Spatial Orientation: Variable Short Penn Line Orientation Test (VSPLOT_TC).

Sustained Attention: Short Penn Continuous Performance Test (SCPT_TPRT).

This analysis was carried out separately for each metric, including SC, FC, and USFC. Furthermore, we repeated the CCA analysis for each cognitive test and applied paired *t*-tests to determine significant differences in the predictive performance of USFC, FC, and SC.

Statistics and reproducibility

In this study, we conducted a series of statistical analyses to explore the relationships between connectivity types and cognitive performance. Initially, we calculated the mean USFC by averaging the values of each pair of connections across the entire sample. A one-sample *t*-test was performed on these averages, with FDR correction applied at a threshold of $p < 0.05$ to account for multiple comparisons.

To examine the relationships between SC and FC, Spearman correlation analyses were conducted at each step, with $p < 0.05$ considered statistically significant. Graph theoretical metrics were computed for each individual across the three metrics: FC, SC, and USFC, allowing for statistical comparisons via *t*-tests. To ensure the robustness and replicability of our model, all measurements were repeated using an alternative atlas (Destrieux).

Additionally, we performed CCA, focusing on the top ten most heavily used segments identified through the USFC model, alongside cognitive assessments available in the HCP dataset. The CCA was executed using the cancor function in R, which identifies pairs of canonical variables that optimally represent the relationships between the top ten USFC measures and cognitive performance scores. We repeated the CCA analysis for each cognitive test and applied paired *t*-tests to determine significant differences in the predictive performance among USFC, FC, and SC.

Finally, while the current CCA analysis provides valuable insights into the relationships between USFC and cognitive performance, future formal predictive analyses incorporating cross-validation methods may enhance our understanding of the generalizability of the detected brain-behavior relationships.

Reporting summary

Further information on research design is available in the Nature Portfolio Reporting Summary linked to this article.

Data availability

The HCP data, including MRI and cognitive assessments analyzed in the current study, are publicly available at http://www.humanconnectome.org.

Code availability

A custom MATLAB code for construction of unified structural and functional connectivity is available online[102] (https://github.com/ArzuHas/USFC.git).

Received: 1 April 2024; Accepted: 28 October 2024;
Published online: 09 November 2024

References

1. Basser, P. J. & Jones, D. K. Diffusion-tensor MRI: theory, experimental design and data analysis—a technical review. *NMR Biomed.***15**, 456–467 (2002).
2. van den Heuvel, M. P. & Hulshoff Pol, H. E. Exploring the brain network: a review on resting-state fMRI functional connectivity. *Eur. Neuropsychopharmacol.* **20**, 519–534 (2010).
3. Sporns, O., Tononi, G. & Kötter, R. The human connectome: a structural description of the human brain. *PLOS Comput. Biol.* **1**, e42 (2005).
4. Hagmann, P. et al. Mapping the structural core of human cerebral cortex. *PLoS Biol.* **6**, e159 (2008).
5. Roberts, J. A. et al. The contribution of geometry to the human connectome - [scite report]. *Neuroimage* **124**, 379–393 (2016).
6. Biswal, B., Yetkin, F. Z., Haughton, V. M. & Hyde, J. S. Functional connectivity in the motor cortex of resting human brain using echo-planar MRI. *Magn. Reson. Med.* **34**, 537–541 (1995).
7. Biswal, B. Resting state fMRI: a personal history. *Neuroimage* **62**, 938–944 (2012).
8. Hebb, D. (Wiley, New York, 1949).
9. Friston, K. J. et al. Psychophysiological and modulatory interactions in neuroimaging. *Neuroimage* **6**, 218–229 (1997).
10. Lowe, M. J., Mock, B. J. & Sorenson, J. A. Functional connectivity in single and multislice echoplanar imaging using resting-state fluctuations. *Neuroimage* **7**, 119–132 (1998).
11. Cordes, D. et al. Frequencies contributing to functional connectivity in the cerebral cortex in "resting-state" data. *AJNR Am. J. Neuroradiol.* **22**, 1326–1333 (2001).
12. Fox, M. D. et al. The human brain is intrinsically organized into dynamic, anticorrelated functional networks. *Proc. Natl Acad. Sci. USA* **102**, 9673–9678 (2005).
13. Greicius, M., Krasnow, B., Reiss, A. & Menon, V. Functional connectivity in the resting brain: a network analysis of the default mode hypothesis. *Proc. Natl Acad. Sci. USA* **100**, 253–258 (2003).
14. Seeley, W. W. The salience network: a neural system for perceiving and responding to homeostatic demands. *J. Neurosci.* **39**, 9878–9882 (2019).
15. Power, J. D., Fair, D. A., Schlaggar, B. L. & Petersen, S. E. The development of human functional brain networks. *Neuron* **67**, 735–748 (2010).
16. Bullmore, E. & Sporns, O. Complex brain networks: graph theoretical analysis of structural and functional systems. *Nat. Rev. Neurosci.* **10**, 186–198 (2009).
17. Gilson, M. et al. Network analysis of whole-brain fMRI dynamics: a new framework based on dynamic communicability. *Neuroimage* **201**, 116007 (2019).
18. Bassett, D. S. & Bullmore, E. T. Small-world brain networks revisited. *Neuroscientist* **23**, 499–516 (2017).
19. Van Den Heuvel, M. P., Bullmore, E. T. & Sporns, O. Comparative connectomics. *Trends Cogn. Sci.* **20**, 345–361 (2016).
20. Heuvel, M. P. V. D. & Sporns, O. Network hubs in the human brain - [scite report]. *Trend Cogn. Sci.* **17**, 683–96 (2013).
21. Adachi, Y. et al. Functional connectivity between anatomically unconnected areas is shaped by collective network-level effects in the macaque cortex. *Cereb. Cortex* **22**, 1586–1592 (2012).
22. Sanz-Leon, P., Knock, S. A., Spiegler, A. & Jirsa, V. K. Mathematical framework for large-scale brain network modeling in the virtual brain. *Neuroimage* **111**, 385–430 (2015).
23. Manos, T. et al. Enhanced simulations of whole-brain dynamics using hybrid resting-state structural connectomes. *Front. Comput. Neurosci.* https://doi.org/10.3389/fncom.2023.1295395 (2023).

24. Esfahlani, F. Z., Faskowitz, J., Slack, J., Misic, B. & Betzel, R. F. Local structure-function relationships in human brain networks across the lifespan. *Nat Commun.* **13**, 2053 (2022).
25. Mišić, B. et al. Network-level structure-function relationships in human neocortex. *Cereb. Cortex* **26**, 3285–3296 (2016).
26. Damoiseaux, J. S. Effects of aging on functional and structural brain connectivity. *Neuroimage* **160**, 32–40 (2017).
27. Uddin, L. Q., Supekar, K. S., Ryali, S. & Menon, V. Dynamic reconfiguration of structural and functional connectivity across core neurocognitive brain networks with development. *J. Neurosci.* **31**, 18578–18589 (2011).
28. Lim, S. et al. Discordant attributes of structural and functional brain connectivity in a two-layer multiplex network. *Sci. Rep.* **9**, 2885 (2019).
29. Gu, Z. et al. Heritability and interindividual variability of regional structure-function coupling. *Nat. Commun.***12**, 4894 (2021).
30. Liégeois, R., Santos, A., Matta, V., Ville, D. V. D. & Sayed, A. H. Revisiting correlation-based functional connectivity and its relationship with structural connectivity. *Netw. Neurosci.* **4**, 1235–1251 (2020).
31. Damoiseaux, J. S. & Greicius, M. D. Greater than the sum of its parts: a review of studies combining structural connectivity and resting-state functional connectivity. *Brain Struc. Funct.* **213**, 525–533 (2009).
32. Dekking, F. M. *A Modern Introduction to Probability and Statistics: Understanding Why and How* 1st edn, Vol. 488 (Springer Science & Business Media, 2005).
33. Abdelnour, F., Voss, H. U. & Raj, A. Network diffusion accurately models the relationship between structural and functional brain connectivity networks. *Neuroimage* **90**, 335–347 (2014).
34. Griffa, A. et al. Transient networks of spatio-temporal connectivity map communication pathways in brain functional systems. *Neuroimage* **155**, 490–502 (2017).
35. Honey, C. J., Kötter, R., Breakspear, M. & Sporns, O. Network structure of cerebral cortex shapes functional connectivity on multiple time scales. *Proc. Natl Acad. Sci. USA* **104**, 10240–10245 (2007).
36. Neudorf, J., Kress, S. & Borowsky, R. Comparing models of information transfer in the structural brain network and their relationship to functional connectivity: diffusion versus shortest path routing. *Brain Struct. Funct.* **228**, 651–662 (2023).
37. Avena-Koenigsberger, A. et al. Path ensembles and a tradeoff between communication efficiency and resilience in the human connectome. *Brain Struct. Funct.* **222**, 603–618 (2017).
38. Amico, E. et al. Toward an information theoretical description of communication in brain networks. *Netw. Neurosci.* **5**, 646–665 (2021).
39. Zhou, D. et al. Efficient coding in the economics of human brain connectomics. *Netw. Neurosci.* **6**, 234–274 (2022).
40. Mišić, B. et al. Cooperative and competitive spreading dynamics on the human connectome. *Neuron* **86**, 1518–1529 (2015).
41. de Pasquale, F., Della Penna, S., Sporns, O., Romani, G. L. & Corbetta, M. A Dynamic Core Network and Global Efficiency in the Resting Human Brain. *Cereb Cortex* **26**, 4015–4033 (2016).
42. Finn, E. S. et al. Functional connectome fingerprinting: identifying individuals using patterns of brain connectivity. *Nat. Neurosci.* **18**, 1664–71 (2015).
43. Raichle, M. E. et al. A default mode of brain function. *Proc. Natl Acad. Sci. USA* **98**, 676–682 (2001).
44. Buckner, R., Andrews-Hanna, J., Schacter, D., Kingstone, A. & Miller, M. The brain's default network - anatomy, function, and relevance to disease. *Year Cogn. Neurosci. 2008* **1124**, 1–38 (2008).
45. Gusnard, D. A. et al. The default mode network in cognition: a topographical perspective. *Nat. Rev. Neurosci.* **22**, 503–513 (2021).
46. Smallwood, J. et al. The default mode network in cognition: a topographical perspective. *Nat. Rev. Neurosci.* **22**, 503–513 (2021).
47. Elton, A. & Gao, W. Divergent task-dependent functional connectivity of executive control and salience networks. *Cortex* **51**, 56–66 (2014).
48. Elton, A. & Gao, W. Task-positive functional connectivity of the default mode network transcends task domain. *J. Cogn. Neurosci.* **27**, 2369–2381 (2015).
49. Gao, W., Gilmore, J. H., Alcauter, S. & Lin, W. The dynamic reorganization of the default-mode network during a visual classification task. *Front Syst. Neurosci.* **7**, 34 (2013).
50. Gao, W. & Lin, W. Frontal parietal control network regulates the anti-correlated default and dorsal attention networks. *Hum. Brain Mapp.* **33**, 192–202 (2012).
51. Gao, W. et al. Evidence on the emergence of the brain's default network from 2 week-old to 2 year-old healthy pediatric subjects. *Proc. Natl Acad. Sci. USA* **106**, 6790–6795 (2009).
52. Menon, V. 20 years of the default mode network: a review and synthesis. *Neuron* **111**, 2469–2487 (2023).
53. Buckner, R. L. & DiNicola, L. M. The brain's default network: updated anatomy, physiology and evolving insights. *Nat. Rev. Neurosci.* **20**, 593–608 (2019).
54. Weber, S., Aleman, A. & Hugdahl, K. Involvement of the default mode network under varying levels of cognitive effort. *Sci. Rep. Uk* **12**, 6303 (2022).
55. Tomasi, D. & Volkow, N. D. Aging and functional brain networks. *Mol. Psychiatry* **17**, 549–458 (2012).
56. Rocca, M. A., Schoonheim, M. M., Valsasina, P., Geurts, J. J. G. & Filippi, M. Task- and resting-state fMRI studies in multiple sclerosis: From regions to systems and time-varying analysis. Current status and future perspective. *Neuroimage Clin.* **35**, 103076 (2022).
57. Saris, I. M. J. et al. Default mode network connectivity and social dysfunction in major depressive disorder. *Sci. Rep.* **10**, 194 (2020).
58. Adams, J. N. et al. Functional network structure supports resilience to memory deficits in cognitively normal older adults with amyloid-β pathology. *Sci. Rep.* **13**, 13953 (2023).
59. Zhou, J. & Seeley, W. W. Network dysfunction in Alzheimer's disease and frontotemporal dementia: implications for psychiatry. *Biol. Psychiatry* **75**, 565–573 (2014).
60. Spreng, R. N., Stevens, W. D., Chamberlain, J. P., Gilmore, A. W. & Schacter, D. L. Default network activity, coupled with the frontoparietal control network, supports goal-directed cognition. *Neuroimage* **53**, 303–317 (2010).
61. Menon, V. & Uddin, L. Q. Saliency, switching, attention and control: a network model of insula function. *Brain Struct. Funct.* **214**, 655–667 (2010).
62. Hwang, K., Bertolero, M. A., Liu, W. B. & D'Esposito, M. The human thalamus is an integrative hub for functional brain networks. *J. Neurosci.* **37**, 5594–5607 (2017).
63. Halassa, M. M. & Sherman, S. M. Thalamo-cortical circuit motifs: a general framework. *Neuron* **103**, 762–770 (2019).
64. Sherman, S. M. Functioning of circuits connecting thalamus and cortex. *Compr. Physiol.* **7** 713–739 (2017).
65. Shine, J. M. Adaptively navigating affordance landscapes: how interactions between the superior colliculus and thalamus coordinate complex, adaptive behaviour - [scite report]. *Neurosci. Amp. Biobehav. Rev.* **143**, 104921 (2022).
66. Driscoll, M. E., Bollu, P. C. & Tadi, P. *Neuroanatomy, Nucleus Caudate*. (StatPearls Publishing, Treasure Island (FL), 2023).
67. Doi, T., Fan, Y., Gold, J. I. & Ding, L. The caudate nucleus contributes causally to decisions that balance reward and uncertain visual information. *Elife* **9**, e56694 (2020).
68. Çırak, M. et al. The caudate nucleus: its connections, surgical implications, and related complications. *World Neurosurg.* **139**, e428–e438 (2020).
69. Grahn, J. A., Parkinson, J. A. & Owen, A. M. The role of the basal ganglia in learning and memory: neuropsychological studies. *Behavioural. Brain Res.* **199**, 53–60 (2009).

70. Goñi, J. et al. Resting-brain functional connectivity predicted by analytic measures of network communication. *Proc. Natl Acad. Sci. USA* **111**, 833–8 (2014).
71. Murphy, K. & Fox, M. D. Towards a consensus regarding global signal regression for resting state functional connectivity MRI. *Neuroimage* **154**, 169–173 (2017).
72. Zhan, L. et al. The significance of negative correlations in brain connectivity. *J. Comp. Neurol.* **525**, 3251–3265 (2017).
73. Fox, M. D., Zhang, D., Snyder, A. Z. & Raichle, M. E. The global signal and observed anticorrelated resting state brain networks. *J. Neurophysiol.* **101**, 3270–83 (2009).
74. Yeo, B. T. T. et al. The organization of the human cerebral cortex estimated by intrinsic functional connectivity. *J. Neurophysiol.* **106**, 1125–6 (2011).
75. Uddin, L. Q., Kelly, A. M. C., Biswal, B. B., Castellanos, F. X. & Milham, M. P. Functional connectivity of default mode network components: Correlation, anticorrelation, and causality. *Human Brain Mapping* **30**, 625–37(2009).
76. Martinez-Gutierrez, E., Jimenez-Marin, A., Stramaglia, S. & Cortes, J. M. The structure of anticorrelated networks in the human brain. *Front. Netw. Physiol.* **2**, 946380 (2022).
77. Li, J. et al. Topography and behavioral relevance of the global signal in the human brain. *Sci Rep. Uk* **9**, 14286 (2019).
78. Skudlarski, P. et al. Measuring brain connectivity: diffusion tensor imaging validates resting state temporal correlations. *Neuroimage* **43**, 554–561 (2008).
79. Chen, G., Chen, G., Xie, C. & Li, S.-J. *Negative Functional Connectivity and Its Dependence on the Shortest Path Length of Positive Network in the Resting-State Human Brain.* https://home.liebertpub.com/brain (2011).
80. Seguin, C., Sporns, O. & Zalesky, A. Brain network communication: concepts, models and applications. *Nat. Rev. Neurosci.* **24**, 557–574 (2023).
81. SM, S. et al. Network modelling methods for FMRI - PubMed. *Neuroimage* **54**, 875–91 (2011).
82. Hutchison, R. M. et al. Dynamic functional connectivity: promise, issues, and interpretations. *Neuroimage* **80**, 360–378 (2013).
83. Hutchison, R. M., Womelsdorf, T., Gati, J. S., Everling, S. & Menon, R. S. Resting-state networks show dynamic functional connectivity in awake humans and anesthetized macaques. *Hum. Brain Mapp.* **34**, 2154–2177 (2013).
84. Allen, E. A. et al. Tracking whole-brain connectivity dynamics in the resting state. *Cereb. Cortex* **24**, 663–676 (2014).
85. Elton, A. & Gao, W. Divergent task-dependent functional connectivity of executive control and salience networks. *Cortex* **51**, 56–66 (2014).
86. Elton, A. & Gao, W. Task-related modulation of functional connectivity variability and its behavioral correlations. *Hum. Brain Mapp.* **36**, 3260–3272 (2015).
87. Reid, A. T. et al. Advancing functional connectivity research from association to causation. *Nat. Neurosci.* **22**, 1751–1760 (2019).
88. R, S.-R. & MW, C. Combining multiple functional connectivity methods to improve causal inferences - PubMed. *J. Cogn. Neurosci.* **33**, 180–194 (2021).
89. A, Z., A, F. & E, B. On the use of correlation as a measure of network connectivity - PubMed. *Neuroimage.* **60**, 2096–106 (2012).
90. Friston, K. J. Functional and effective connectivity: a review. *Brain Connect.* **1**, 13–36 (2011).
91. Jeurissen, B., Leemans, A., Tournier, J. D., Jones, D. K. & Sijbers, J. Investigating the prevalence of complex fiber configurations in white matter tissue with diffusion magnetic resonance imaging. *Hum. Brain Mapp.* **34**, 2747–2766 (2013).
92. Lucignani, M. et al. Reliability on multiband diffusion NODDI models: a test retest study on children and adults. *Neuroimage* **238**, 118234 (2021).
93. Luca, A. D., Guo, F., Froeling, M. & Leemans, A. Spherical deconvolution with tissue-specific response functions and multi-shell diffusion MRI to estimate multiple fiber orientation distributions (mFODs). *Neuroimage* **222**, 117206 (2020).
94. Fodor, I. K. A survey of dimension reduction techniques. *arXiv* https://doi.org/10.48550/arXiv.1403.2877 (2002).
95. Wold, S., Ruhe, A., Wold, H. & Dunn, I. W. J. The collinearity problem in linear regression. The partial least squares (PLS) approach to generalized inverses. *SIAM J. Sci. Stat. Comput.* **5**, 735–743 (1984).
96. Essen, D. C. V. et al. The WU-minn human connectome project: an overview. *Neuroimage* **80**, 62–79 (2013).
97. Glasser, M. F. et al. The minimal preprocessing pipelines for the human connectome project. *Neuroimage* **80**, 105–124 (2013).
98. Has Silemek, A. C. et al. Functional and structural connectivity substrates of cognitive performance in relapsing remitting multiple sclerosis with mild disability. *Neuroimage Clin.* **25**, 102177 (2020).
99. Behrens, T. E., Berg, H. J., Jbabdi, S., Rushworth, M. F. & Woolrich, M. W. Probabilistic diffusion tractography with multiple fibre orientations: what can we gain? *Neuroimage* **34**, 144–155 (2007).
100. Jeurissen, B., Tournier, J. D., Dhollander, T., Connelly, A. & Sijbers, J. Multi-tissue constrained spherical deconvolution for improved analysis of multi-shell diffusion MRI data. *Neuroimage* **103**, 411–426 (2014).
101. Hochberg, Y. B. Y. Royal statistical society publications. *J. R. Stat. Soc. (Methodological)* **57** https://doi.org/10.1111/j.2517-6161.1995.tb02031.x (1995).
102. Has Silemek, A. C. ArzuHas/USFC: USFC (USFC). *Zenodo* https://doi.org/10.5281/zenodo.13997197 (2024).
103. Hagberg, A., Swart, P. & S Chult, D. *Exploring Network Structure, Dynamics, and Function Using NetworkX.* https://www.osti.gov/biblio/960616 (2008).
104. Bassett, D. & Bullmore, E. Small-world brain networks - PubMed. *Neurosci. Rev. J. bringing Neurobiol. Neurol. Psychiatry* **12**, 512–23 (2006).
105. Latora, V. & Marchiori, M. Efficient behavior of small-world networks. *Phys. Rev. Lett.* **87**, 198701 (2001).
106. Achard, S. & Bullmore, E. Efficiency and cost of economical brain functional networks. *PLoS Comput. Biol.* **3**, e17 (2007).
107. Newman, M. E. J. From the cover: modularity and community structure in networks. *Proc. Natl Acad. Sci. USA* **103**, 8577–8582 (2006).
108. Freeman, L. C. A set of measures of centrality based on betweenness. *Sociometry* **40**, 35–41 (1977).
109. Destrieux, C., Fischl, B., Dale, A. & Halgren, E. Automatic parcellation of human cortical gyri and sulci using standard anatomical nomenclature. *Neuroimage* **53**, 1–15 (2010).
110. González, I., Déjean, S., Martin, P. G. P. & Baccini, A. CCA: An R package to extend canonical correlation analysis. *J. Stat. Softw.* **23** https://doi.org/10.18637/jss.v023.i12 (2008).

Acknowledgements

This work was supported by the National Institutes of Health (R01DA042988 and R01DA043678) and by Cedars-Sinai Precision Medicine Initiative Award and institutional support (to W.G.).

Author contributions

Arzu C Has Silemek: Investigation, Formal analysis, Data Curation, Writing-Original Draft preparation - Review & Editing; Haitao Chen: Formal analysis, Writing - Review & Editing; Pascal Sati: Writing - Review & Editing; Wei Gao: Conceptualization, Investigation, Supervision, Writing - Review & Editing.

Competing interests

The authors declare no competing interests.

Additional information

Supplementary information The online version contains supplementary material available at https://doi.org/10.1038/s42003-024-07160-y.

Correspondence and requests for materials should be addressed to Arzu C. Has Silemek or Wei Gao.

Peer review information *Communications Biology* thanks Emeline Mullier and the other, anonymous, reviewer(s) for their contribution to the peer review of this work. Primary Handling Editors: Aylin Bircan and Johannes Stortz. A peer review file is available.